Part II Applied Physics

Section 1 Atomic, Molecular and Optical Physics

Chapter 1. Quantum Optics and Photonics

Academic and Research Staff

Professor Shaoul Ezekiel, Dr. M. Selim Shahriar

Visiting Scientists and Research Affiliates

Dr. Philip R. Hemmer,[1] Dr. Mara G. Prentiss,[2] Dr. Farhad Zarinetchi,[2] John D. Kierstead[1]

Graduate Students

John J. Donoghue,[3] Daniel Katz,[2] Juliet Mervis,[2] Stephen P. Smith

Undergraduate Students

Arthur Chu[2]

1.1 Optical Data Storage with Raman Excited Spin Echoes

Sponsor

U.S. Air Force - Electronic Systems Division
Contract F19628-92-K-0013

There has been much recent interest in the use of optical photon echoes for information storage and processing.[4] So far, however, the most successful demonstrations have been restricted to doped crystals operating at liquid helium temperatures, and homogeneous decay of the excited state limits performance. Here we demonstrate, theoretically as well as experimentally, that optical data can be stored and retrieved using spin echoes which are excited and detected by the optical resonance Raman interaction. The advantage is that spin echoes contain no contribution from the optical excited state and therefore are not limited by excited state decay. Moreover, since Raman spin echoes are optically excited and detected, full optical holographic spatial resolution is available. Finally, it might be possible to develop high temperature optical memories and processors, since spin echo data storage has been demonstrated at room temperature.[5]

The ability of Raman excited spin coherence to store optical temporal and phase information is based on the fact that this coherence is sensitive to the relative phases of the optical fields.[6] When inhomogeneous broadening is present, the differential optical phase sensitivity permits the storage of optical temporal variations, just as in conventional optical (or microwave) echo storage schemes.

Experimental realization of the three-part storage and recall scheme is accomplished with a sodium atomic beam that has three spatially separated interaction zones and uses an off-resonant optical-Raman beam as the rephasing field. The experimental setup is illustrated in figure 1. Here, the Raman transition is the

$$3^2S_{1/2}(F=1,m=1)\leftrightarrow$$

$$3^2P_{1/2}(F=2,m=2)\leftrightarrow 3^2S_{1/2}(F=2,m=1)$$

---

1 Rome Laboratory, Hanscom, Massachusetts.

2 Harvard University, Cambridge, Massachusetts.

3 Tufts University, Medford, Massachusetts.

4 M.K. Kim and R. Kachru, "Storage and Phase Conjugation of Multiple Images Using Backward-stimulated Echoes in Pr^{3+} :LaF_3," *Opt. Lett.* 12: 593 (1987).

5 S. Fernbach and W.G. Proctor, "Spin-echo Memory Device," *J. Appl. Phys.* 26: 170 (1955).

6 M.S. Shahriar and P.R. Hemmer, "Direct Excitation of Microwave-spin Dressed States Using a Laser-excited Resonance Raman Interaction," *Phys. Rev. Lett.* 65: 1865 (1990).

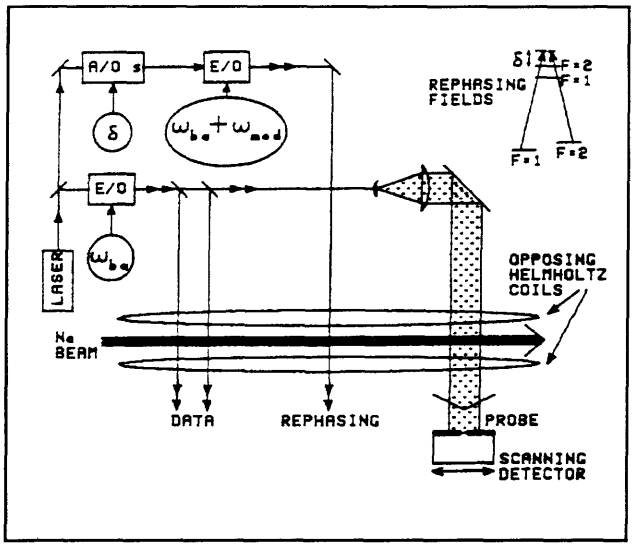

Figure 1. Experimental setup for optical data storage and recall using optical-Raman excited spin echoes, in a sodium atomic beam.

transition at 589.7 nm optical frequency, where the ground state splitting is 1.772 GHz and the excited state decay time is 16 nsec. Ground state inhomogeneous broadening is produced using the linear Zeeman shift and an applied magnetic field gradient of 1 Gauss/cm, to give a total ground state inhomogeneous broadening of 450 kHz.

The optical pulse sequence is shown in figure 2a. The first two Raman pulses interfere to store the optical temporal information via spectral hole-burning. The rephasing is accomplished with an off-resonance Raman π-pulse. The Raman probe beam senses the echo via changes in absorption. Figure 2b shows the experimentally observed echo signals. The echo amplitude is about 50% of the maximum demodulated signal obtained when a single, saturating Raman data pulse is applied in the absence of a magnetic field gradient (no dephasing). Figure 2c shows the theoretical echo signal calculated using a numerical solution of the optical Bloch equations for input parameters that approximately correspond to experimental conditions of figure 2c. Good qualitative agreement between theory and experiment is achieved, both in the width and peak amplitude of the echo signals.

Although the present optical data storage experiment employs optical data pulses that are longer than the excited state homogeneous decay time, this is not a fundamental requirement. In fact, Raman resonant optical pulses shorter than the optical homogeneous decay time can also be stored. The new fundamental limit on optical storage capacity, using Raman-optical echoes, is given by the ratio of the spin homogeneous lifetime to the optical inhomogeneous lifetime. This is typically several orders of magnitude larger than for optical two-level echoes. Furthermore, if the rephasing microwave π-pulse is split into two temporally separated π/2-pulses, then archival storage is possible.

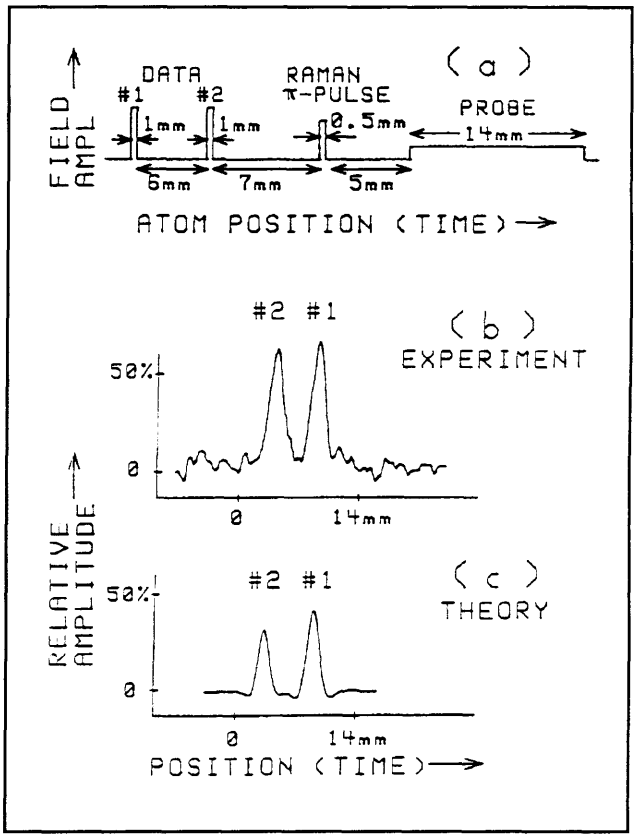

Figure 2. (a) Pulse sequence for data storing and retrieval. (b) Experimentally observed echo signals. (c) Corresponding theoretical echoes.

In summary, we have experimentally demonstrated that the Raman transparent states can store and retrieve optical temporal and phase information via a ground state spin echo process. This opens up the possibility of enhancing the performance of optical photon echo memories. Future work includes demonstration of this type of data storage in cryogenic doped crystals as well as a search for higher temperature materials.

1.2 Phase-dependent Velocity Selective Coherent Population Trapping in a Folded Three-level Λ System under Standing Wave Excitation

Sponsors

U.S. Air Force - Electronic Systems Division
Contract F19628-92-K-0013

U.S. Navy - Office of Naval Research
Grant N0014-91-J-1808

Recently, there has been a great deal of interest in the forces experienced by a folded three-level Λ atom. Aspect et al.[7] first demonstrated that such an atom can be cooled below the recoil limit via velocity selective coherent population trapping (VSCPT) when excited by a pair of counter-propagating traveling waves. Here, we show theoretically that VSCPT occurs in a Λ atom excited by a pair of Raman resonant standing waves, and its efficiency depends on the relative phase, ϕ, between the standing waves. Finally, we describe briefly the generalization of this process to three dimensions.

The importance of VSCPT in Raman resonant standing waves stems from our earlier experimental observation of deflection and cooling of Λ sodium atoms in an atomic beam.[8] This experiment suggests that these standing wave forces could be used to design a stimulated force trap. In addition, our theory predicts that the cooling can be made to have characteristics very similar to those of conventional polarization gradient cooling (see next section), so that such a trap should have a sub-Doppler temperature. The theory presented here suggests that it may be possible to reach a sub-recoil temperature in a Raman force trap.

In analogy to the traveling wave VSCPT, we are interested in finding a state (the dark state) which satisfies the following conditions: (1) it does not contain any excited states so that it is completely decoupled from the vacuum fields, and (2) the net amplitude for coupling this state to any of the excited states must vanish. Let us denote the linear momentum of the atom by p and the wavenumber of the optical field by k. It can be shown that if $p = 0$ and/or $\phi = 0$ then the state:

$$|NC(p)> = \frac{1}{2}$$

$$[|a, p - \hbar k> \exp(-i\phi) + |a, p + \hbar k>$$

$$\exp(i\phi) - |b, p - \hbar k> - |b, p + \hbar k>]$$

does not couple to any excited state, as illustrated in figure 3. Here, the square boxes represent the relative transition matrix elements. Summing over the allowed transitions we find, for an atom starting in $|NC>$ at $t = 0$, that the amplitude of being in the excited state after a time dt is given by $dA_e \cong -2i(dt)^2 gk(p/m) \sin\phi$, where g is the Rabi frequency, and m is the mass of the atom. Thus, for $p = 0$ and/or $\phi = 0$, $|NC>$ is a dark state. For $\phi \neq 0$, we therefore have a single, zero velocity dark state, and VSCPT occurs. The efficiency of VSCPT would vary as $\sin^2\phi$, being maximum at $\phi = (2n+1)\pi/2$ and vanishing at $\phi = n\pi$. We also find that for $\phi = (2n+1)\pi/2$, the standing wave VSCPT is nearly as efficient as the traveling wave.

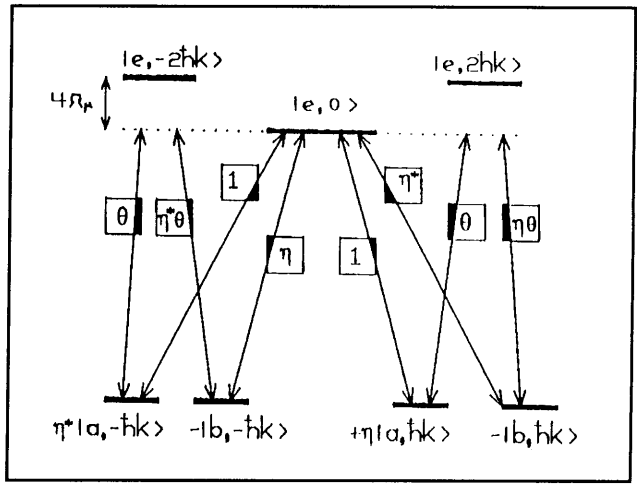

Figure 3. Illustration of the dark state, $|NC(0)>$. Here, $\eta \equiv \exp(i\phi)$, and $\theta \equiv \exp(i\Omega_r t)$. The numbers in the boxes represent the relative weights of the matrix element. Here, we have chosen $\delta = -\Omega_r$.

The existence of VSCPT corresponds to the absence of diffusion for zero velocity atoms in the trapped state. However, Chang et al.[9] have previously computed a non-zero diffusion coefficient in Raman resonant standing waves by a perturbative numerical solution of the Wigner density matrix equation of motion. This disagreement with Chang et al. seems to stem from the fact that they assumed, *a priori*, that the distribution of atoms in momentum space is smooth, which is in sharp contrast with the result of VSCPT. We should also point out that VSCPT observed by Aspect et al. for a variable angle between the planes of polarization of two counterpropagating traveling waves can be interpreted in terms of the theory of standing wave VSCPT as developed here, thus validating our

---

7 A. Aspect, E. Arimondo, R. Kaiser, N. Vansteenkiste, and C. Cohen-Tannoudji, *Phys. Rev. Lett.* 61: 826 (1988).

8 P. Hemmer, M. Shahriar, M. Prentiss, D. Katz, K. Berggren, J. Mervis and N. Bigelow, *Phys. Rev. Lett.* 68: 3148 (1992).

9 S. Chang, B. Garraway, and V. Minogin, *Opt. Comm.* 77: 19 (1990).

result. Finally, we have found that this process can be generalized to three dimensions employing a $j = 1 \leftrightarrow j' = 1$ transition, with three mutually orthogonal pairs of Raman resonant standing waves.

In summary, we have shown theoretically that phase sensitive VSCPT takes place when a Λ system is excited by a pair of Raman resonant standing waves. This corresponds to absence of diffusion for zero velocity atoms in the trapped state, in disagreement with predictions made by Chang et al. We also find that previous experimental observations reported by Aspect et al. agree with our predictions. Finally, we outline the generalization to three dimensions. Given our prior observation of stimulated trapping and cooling forces and our theoretical prediction of strong pol-grad cooling in Raman resonant standing waves, the simultaneous existence of VSCPT may make it possible to design a subrecoil temperature trap for Λ atoms.

1.3 Continuous Pol-Grad Pre-Cooling for Loading a Subrecoil Temperature Trap

Sponsors

U.S. Air Force - Electronic Systems Division
Contract F19628-92-K-0013
U.S. Navy - Office of Naval Research
Grant N0014-91-J-1808

As discussed in the preceding section, there has been increasing interest in multilevel atoms that undergo velocity selective coherent population trapping (VSCPT) into a zero velocity dark state. However, since VSCPT takes place via a random walk in momentum space, in three dimensions the efficiency would fall off rapidly as a function of velocity, with a capture range of the order of the recoil velocity. Therefore, in order to significantly populate the 3D dark state, it is necessary to pre-cool atoms to the recoil limit. It is advantageous for this pre-cooling to occur simultaneously with VSCPT; otherwise the random walk causes most of the atoms to heat up to velocities beyond the capture range. This type of pre-cooling does not exist in the various VSCPT schemes considered so far.

Here, we present a new mechanism under which polarization-gradient cooling efficiently slows atoms from a sample at the Doppler limit to the recoil limit. Unlike other methods of cooling to the recoil limit, this cooling occurs under the same conditions as required for VSCPT. We illustrate the basic mechanism in one dimension using a Sisyphus model. The predictions of this model are consistent with numerical results obtained from continued fractions as well as from numerical integrations of the optical Bloch equations. We also discuss the generalization of this scheme to three dimensions. This new mechanism opens the possibility of continuously cooling a large number of atoms to a subrecoil temperature.

The basic features of this cooling technique are well demonstrated in one dimension by a Λ system excited by a pair of Raman resonant standing wave fields. Efficient cooling is obtained in the case where the common mode detuning δ is positive and the phase difference ϕ between the standing waves is $\pi/4$. We have developed a Sisyphus type model to interpret this process physically. This model is illustrated in figure 4, using the non-absorbing ($|->$) and absorbing ($|+>$) superposition states. Figure 4a shows the Rabi frequencies, figure 4b shows the population of $|+>$, and figure 4c shows the Stark shifts of $|+>$ and $|->$. As can be seen, the atoms on average climb energy hills, thus experiencing cooling.

Figure 5a (thick line) shows a plot of the averaged force in natural units as a function of velocity obtained from a continued fraction solution. The parameters used here are $\phi = \pi/4$, $g_0 = 0.3$ and $\delta = 1.0$. We fit this plot to a function of the form $f(v) = -\zeta_0 \cdot v/(1 + v^2/v_c^2)$, which is maximum at $v = v_c$. We find $v_c \cong 5.5 \times 10^{-3}$ and $\zeta_0 \cong 0.81$.

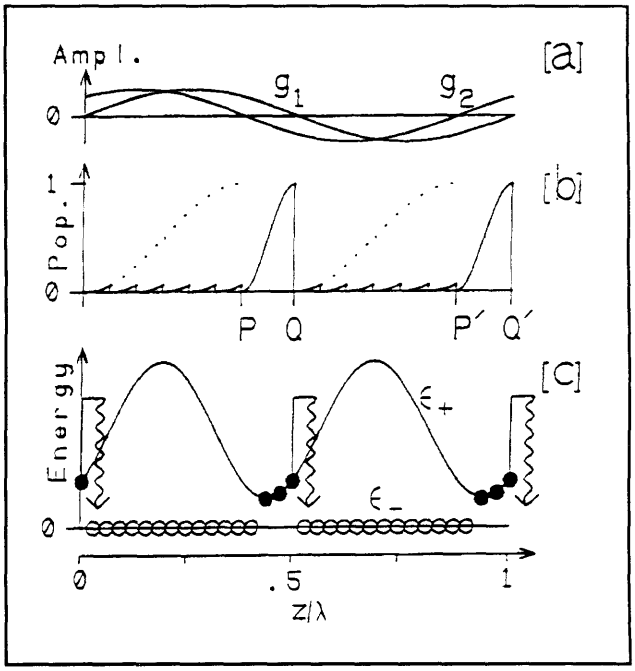

Figure 4. (a) Rabi frequencies for $\chi = \pi/4$. (b) Population of the $|W>$ state for a moving atom. (c) Sisyphus cooling.

The Sisyphus type model predicts $v_c = 3.4 \times 10^{-3}$ and $\zeta_0 \cong 0.97$, with reasonable agreement. For equivalent values of parameters, these numbers are comparable ($\zeta_0 = 3.0$, $v_c = 4.0 \times 10^{-3}$) to the ones estimated by Dalibard et al.[10] for a J = 1/2 $\leftrightarrow$J' = 3/2 transition. The dashed line superimposed on figure 5a shows the corresponding values of the Doppler cooling force, calculated for the $|a> \leftrightarrow |e>$ transition, in the absence of $|b>$, for the same parameters. As can be seen, the pol-grad cooling coefficient (slope) is about a factor of 30 larger than the Doppler cooling coefficient. Figure 5b shows how the force varies as a function of ϕ, for $v = 5.5 \times 10^{-3}$.

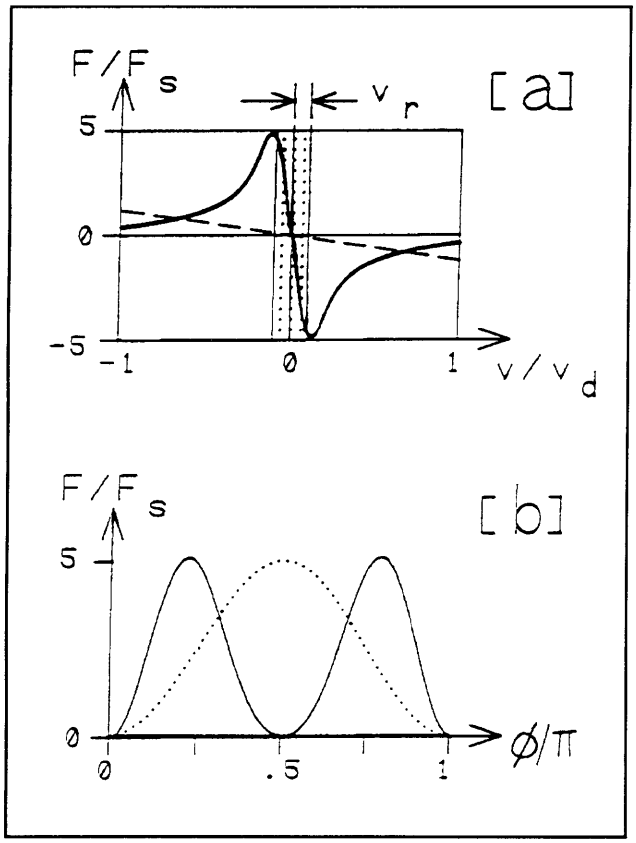

Figure 5. (a) The thick line shows the averaged pol-grad cooling force for sodium as a function of velocity, in units of $F_s = 10^{-3} \times \hbar k\Gamma/2$. The dashed line shows the corresponding Doppler cooling force, and the dotted area represents the capture range for VSCPT. (b) The solid line shows the pol-grad cooling force as a function of ϕ. The dotted line shows the efficiency of VSCPT.

As discussed above, this system undergoes VSCPT into a zero velocity dark state, so that the equilibrium temperature is limited only by the interaction time and can be substantially below the recoil limit. The efficiency of VSCPT into this state varies as $\sin^2\phi$, as illustrated by the dotted line in figure 5b. We have also found how to generalize this scheme to three dimensions, following the approach of Ol'shanii et al.[11]

We have estimated the enhancement of the efficiency of VSCPT in three dimensions due to the pol-grad pre-cooling. Consider, for example, a sample of sodium atoms cooled to the Doppler limit. In the presence of the pol-grad cooling mechanism, the atoms would be pre-cooled to a velocity spread of the order of v_r, so that the time needed for all the atoms to end up in the dark state would be much less than that needed in the absence of such pre-cooling. Preliminary calculations suggest nearly three orders of magnitude enhancement in efficiency from pol-grad pre-cooling.

In summary, we show that pol-grad cooling occurs in the Λ system simultaneously with VSCPT. This process may continuously and efficiently transfer atoms from a Doppler temperature sample to near-recoil velocities that are within the capture range of VSCPT, which would then continuously cool the atoms to below the recoil limit. This pol-grad pre-cooling is estimated to enhance the VSCPT pumping rate by nearly three orders of magnitude compared to the rate achievable from Doppler pre-cooling alone. We present results from a Sisyphus model, along with numerical results obtained from continued fractions. Experimental efforts are in progress for realizing this scheme in three dimensions.

1.4 Raman Gain in a Λ Three-level System with Closely Spaced Ground States

Sponsor

U.S. Air Force - Electronic Systems Division
Contract F19628-92-K-0013

Recently, there has been much interest in the Raman gain observed in a Λ system with closely spaced ground states such that both ground states are initially equally populated and are both coupled

[10] J. Dalibard and C. Cohen-Tannoudji, *J. Opt. Soc. Am. B* 6: 2023 (1989).

[11] M. Ol'shanii and V. Minogin, In *Proceedings of the International Workshop on Light Induced Kinetic Effects on Atoms, Ions, and Molecules,* ed. L. Moi et al. (Pisa, Italy: ETS Editrice, 1991), p. 99.

to the excited state by a single frequency pump.[12] This system is of interest for applications such as frequency shifting,[13] self phase conjugation,[14] and high precision laser magnetometry.

We have studied the mechanism of this gain and found qualitative agreement with experimental results.[15] Briefly, a single frequency pump interacts with both legs of the system, as shown in figure 6a. Figure 6b shows a typical gain lineshape. The vertical rectangle superimposed on this plot indicates a resonance frequency of the dressed states of the atom and the pump. As can be seen, gain is peaked at this resonance frequency. Thus, we are able to interpret the gain spectrum in terms of the energy intervals of the dressed states of the pumped system.

The gain mechanism is analogous to the process of sideband amplification in a strongly driven two-level system. However, the width of gain is not limited by the linewidth of the excited state. This is illustrated in figure 6c, where the linewidth is plotted as a function of pump Rabi frequency. As can be

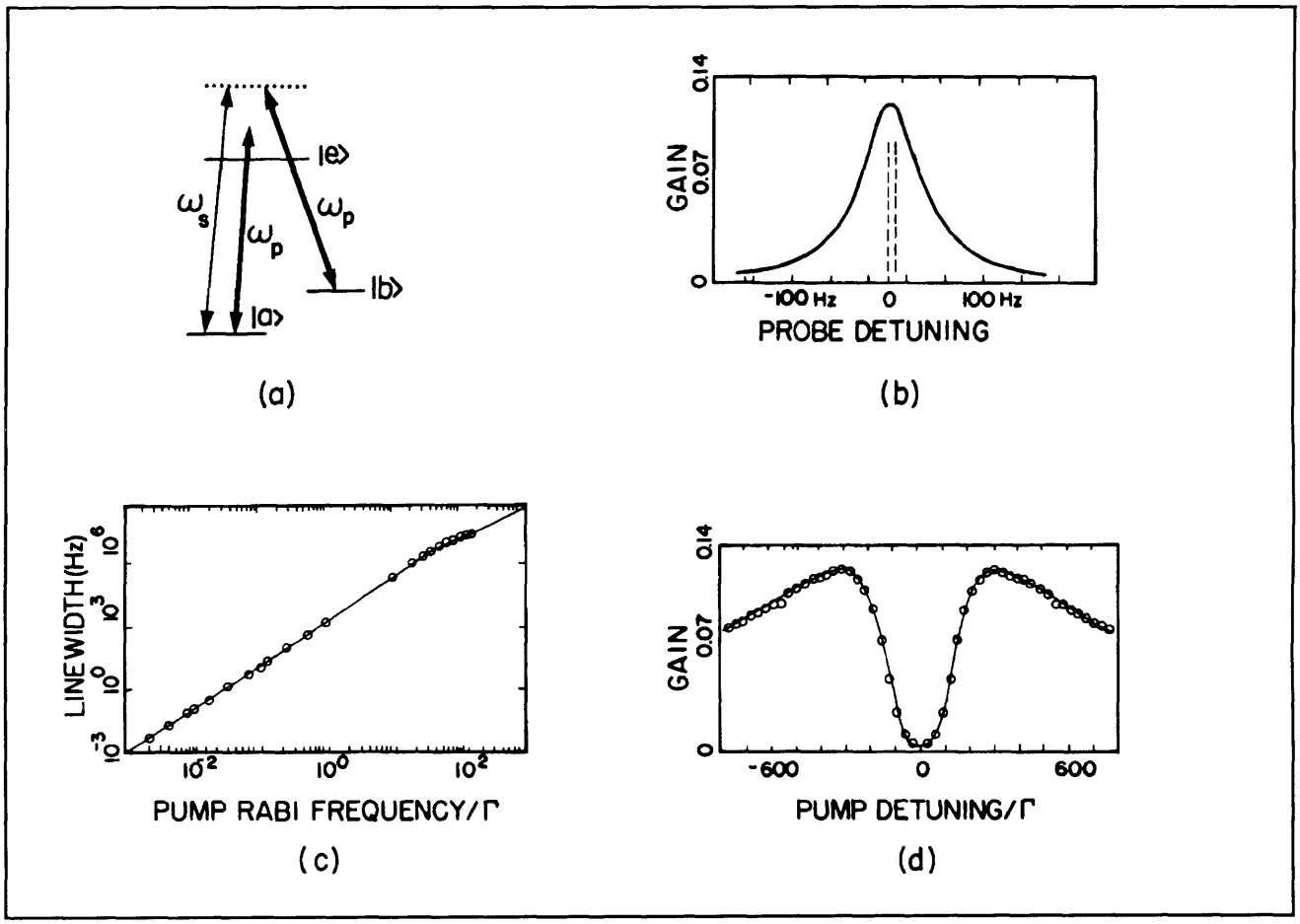

Figure 6. (a) Doubly pumped Raman gain scheme. (b) A typical gain lineshape, centered at a resonance frequency of the dressed states. (c) Linewidth of gain as a function of pump Rabi frequency. (d) Gain as a function of pump detuning. The gain is expressed in arbitrary units.

---

[12] J. Donoghue, M. Cronin-Golomb, J.S. Kane, and P.R. Hemmer, *Opt. Lett.* 16: 1313 (1991); M. Poelker and P. Kumar, *Opt. Lett.* 17(6): 399 (1992); M.S. Shahriar, P.R. Hemmer, J. Donoghue, M. Cronin-Golomb, and P. Kumar, *OSA Annual Meeting Tech. Dig.* 23: 127 (1992).

[13] M. Poelker and P. Kumar, *Opt. Lett.* 17(6): 399 (1992).

[14] J. Donoghue, M. Cronin-Golomb, J.S. Kane, and P.R. Hemmer, *Opt. Lett.* 16: 1313 (1991).

[15] M. Poelker and P. Kumar, *Opt. Lett.* 17(6): 399 (1992); M.S. Shahriar, P.R. Hemmer, J. Donoghue, M. Cronin-Golomb, and P. Kumar, *OSA Annual Meeting Tech. Dig.* 23: 127 (1992).

seen, linewidth falls off linearly with the Rabi frequency. In practice, linewidth is limited only by additional factors such as transit time. This is consistent with extremely narrow gains (less than 1 kHz) observed in sodium vapor. In addition, we have found that gain amplitude becomes a constant below a certain intensity. Thus, this gain mechanism is in principle thresholdless (if not limited by transit time). This is because the dressed states population inversion needed for this gain is created via optical pumping. Thus, for a long enough transit time, optical pumping saturates even for a very low pump intensity.

In summary, we have studied the Raman gain mechanism for a doubly pumped Λ system. For a low intensity, the gain amplitude and width are limited by transit time only. These observations are in qualitative agreement with previous experimental observations. One of the various applications of this process is high resolution laser magnetometry. We have performed preliminary experiments for this application, with encouraging results.

1.5 Brillouin Laser Fiberoptic Gyroscope

Sponsor

Charles S. Draper Laboratory
Contract DL-H-418522

Research is in progress on a new fiberoptic ring laser gyroscope based on two counter-propagating stimulated Brillouin scattering (SBS) lasers which are generated in the same fiberoptic ring resonator.[16] The use of SBS is crucial to the operation of this gyro because a conventional solid-state gain medium cannot support simultaneous bidirectional lasing due to gain competition. It is the directional property of the SBS gain medium that prevents gain competition and thus allows stable, simultaneous, bidirectional lasing.

In the presence of an inertial rotation normal to the plane of the resonator, a difference frequency is automatically generated between the counterpropagating SBS lasers which is directly proportional to the rotation rate,[17] as predicted by the Sagnac effect. The operation of this gyro is very similar to that of the bulkoptic ring laser gyroscope (RLG) based on the He-Ne gain medium. It should be noted that gain competition in a gaseous medium is avoided by using two partially overlapping, Doppler broadened gain media.

In contrast with the passive interferometer or resonator gyroscope, the SBS fiber RLG, as in the bulkoptic RLG, does not require external means to measure the nonreciprocal phase shift that is induced by rotation.

Figure 7 shows a simplified schematic of a SBS ring laser gyroscope. Light from a 1 mW He-Ne laser at 1.15 μm is split into two pump beams, P1 and P2, shifted by acousto-optic modulators, and coupled into counterpropagating directions of the same ring resonator. For maximum effective pump power inside the resonator, the pump lasers are held at the center of a cavity resonance, using a servo not shown in the figure, and are matched to the polarization of the cavity resonance.

With the pump lasers P1 and P2 above the 60 μW Brillouin threshold, two SBS lasers, B1 and B2, are generated simultaneously in directions opposite to those of their respective pumps. The two SBS lasers are then combined via a coupler and fall onto detector D.

Figure 8 shows the difference frequency between B1 and B2 when a sinusoidal rotation is applied to the gyroscope. As predicted by the Sagnac effect, the frequency difference varies linearly with the applied rotation rate, which is 90 degrees out of phase with the rotation angle in figure 8b.

However, it is important to note that, in figure 8, for a range of low rotation rates the frequency differ-

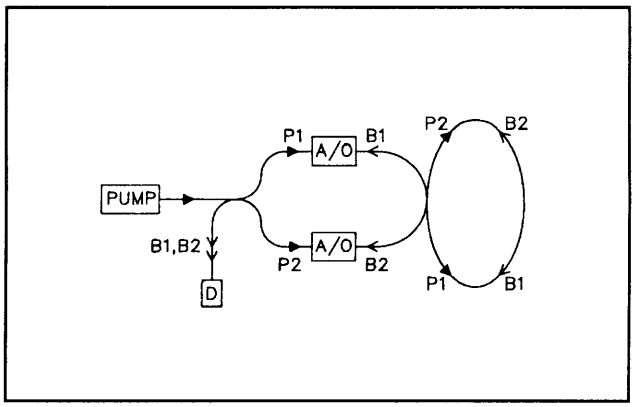

Figure 7. Simplified schematic diagram for a SBS ring laser gyroscope.

[16] S.P. Smith, F. Zarinetchi, and S. Ezekiel, "Fiberoptic Ring Laser Gyroscope," *Proceedings of OFS '89,* Paris, France, 1989, post deadline paper.

[17] F. Zarinetchi, S.P. Smith, and S. Ezekiel, "Stimulated Brillouin Fiber Optic Laser Gyroscope," *Opt. Lett.* 16: 229 (1991).

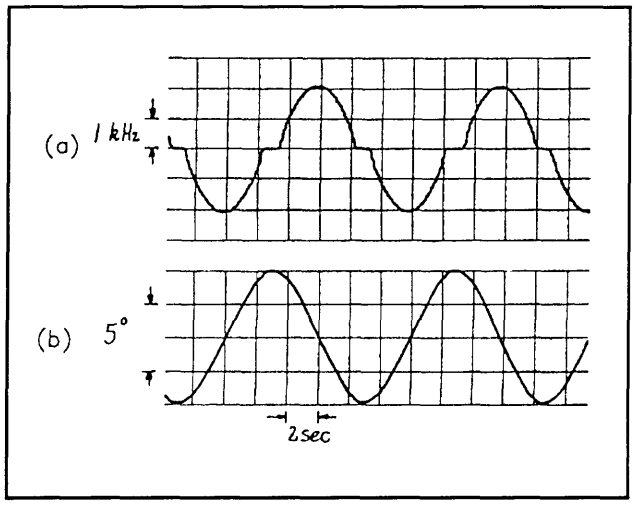

Figure 8. Simultaneous recording of (a) difference frequency between SBS lasers as a function of rotation and (b) angle of the applied rotation.

ence between the SBS lasers is zero. This "lock-in'" zone is similar to that observed in the bulkoptic RLG and is caused by the coupling of the counterpropagating lasers through backscattering within the cavity. In the bulkoptic RLG, the lock-in effect has been thoroughly studied and is removed by mechanical dither.[18]

Mechanical rotation dither minimizes the amount of time that the gyro spends in the lock-in zone, thus reducing the errors due to lock-in. Mechanically dithering the fiber RLG would be much simpler than dithering the bulkoptic RLG because of its very small mass.

Another promising method for the removal of lock-in, which is being investigated here and elsewhere,[19] is optical dither. In this case, instead of mechanically rotating the cavity, the optical path length of the cavity is modulated to generate a nonreciprocal phase shift between the SBS lasers. The optical path length of the cavity can be modulated using two phase shifters, PS1 and PS2, symmetrically located on the cavity, as shown in figure 9. With the phase shifters driven 180 degrees out of phase, there is no net change in the optical length of the cavity. However, due to the finite time it takes the light to go from one modulator to the other, a small nonreciprocal phase shift is generated. By appropriately adjusting the phase modulations, the

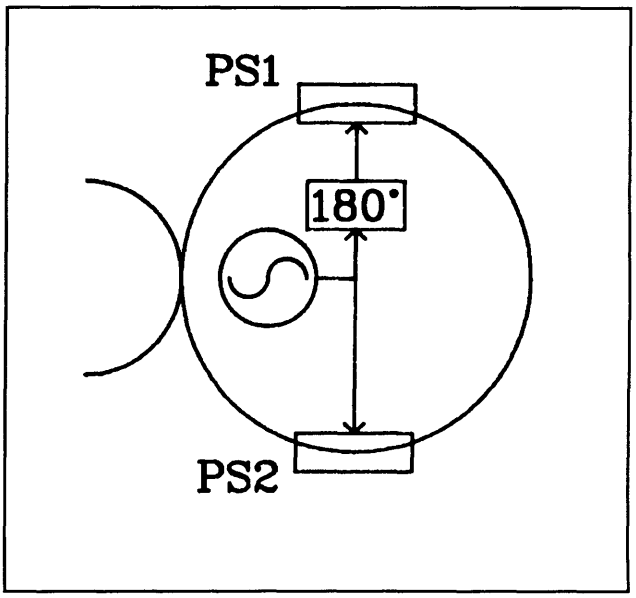

Figure 9. Simplified schematic diagram of a fiber resonator with optical dither.

coupling between the lasers can be greatly suppressed or completely eliminated.

Figures 10 and 11 demonstrate the effect of adjusting optical dither in a fiber cavity with high backscattering. Figure 10a shows the difference in frequency between the SBS lasers for a peak rotation equivalent to a Sagnac frequency of approximately 9 kHz and a lock-in zone of about 1 kHz, with Figure 10b indicating the corresponding rotation angle. Figure 11 shows the response to the same rotation with reduced optical dither, thus increasing the size of the lock-in zone to approximately 2 kHz. In practice, the maximum achievable lock-in suppression is limited by several factors including errors in modulator location, misadjustment of modulation parameters, and modulation distortion.

Another method for removing the lock-in is by generating the SBS lasers with a large frequency difference between them to prevent the lasers from locking. It is possible to generate a separation in frequency between the SBS lasers by either frequency shifting one of the pump lasers or by using separate pumps. In this way, the counterpropagating SBS lasers can be generated in different longitudinal modes of the cavity. Figure 12

[18] F. Aronowitz, "The Laser Gyro," in *Laser Applications,* ed. M. Ross (New York: Academic Press, 1971), vol. 1, pp. 133-200.

[19] S. Huang, K. Toyama, P.A. Nicati, L. Thevenaz, B.Y. Kim, and H.J. Shaw, "Brillouin Fiber Optic Gyro with Push-pull Phase Modulator and Synthetic Heterodyne Detection," *Proc. SPIE* 1795 (1992), Fiber Optic and Laser Sensors X, Boston, Massachusetts, September 8-11, 1992.

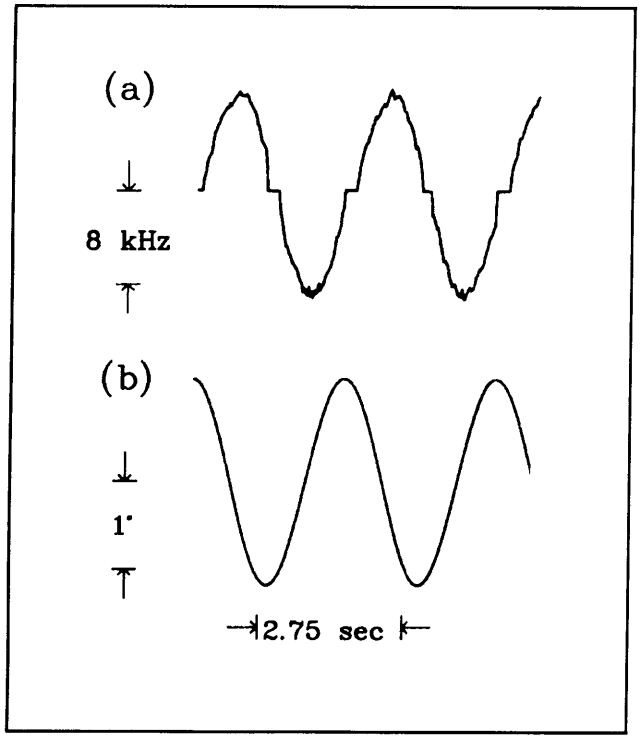

Figure 10. (a) Recording of SBS laser difference frequency and (b) the corresponding rotation angle with applied optical dither.

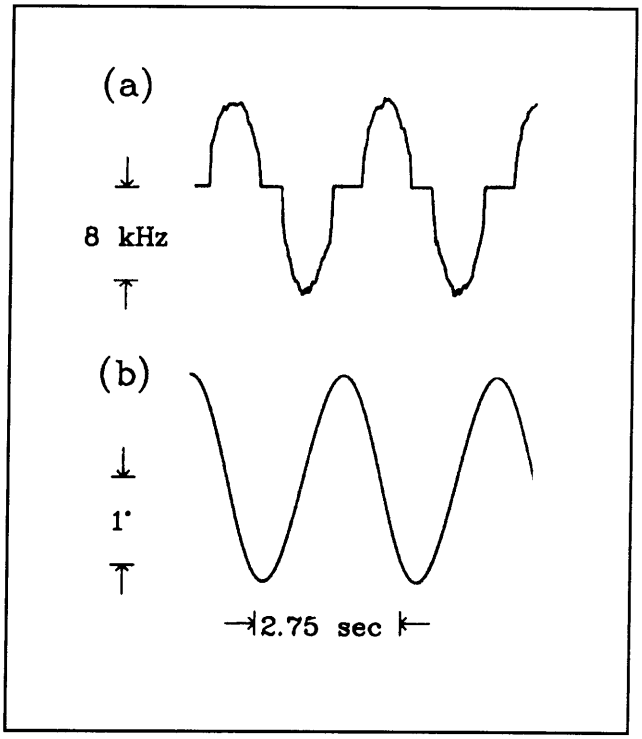

Figure 11. (a) SBS laser difference frequency and (b) the corresponding rotation angle with reduced optical dither.

shows the lock-in free output beat frequency with rotation for such a configuration.

Aside from the temperature sensitivity of this mode of operation, there are a number of additional error sources that are unique to such an SBS gyro. One such error is due to bias variations caused by SBS dispersion pulls. In this case, the backscattering of pump laser P1, for example, generates a very small SBS gain in the same direction as P1. This new SBS gain, however, is also in the same direction as SBS laser B2 and will pull the frequency of B2, causing a bias variation. Further, since the backscattering in the cavity is highly variable, the size of the new SBS gain and hence the size of this frequency pull will also be highly variable.

In addition to lock-in, there are other error sources that are unique to any type of fiber resonator gyro. These include fiber birefringence and the nonlinear optical Kerr effect,[20] both of which have been observed and must be appropriately controlled.

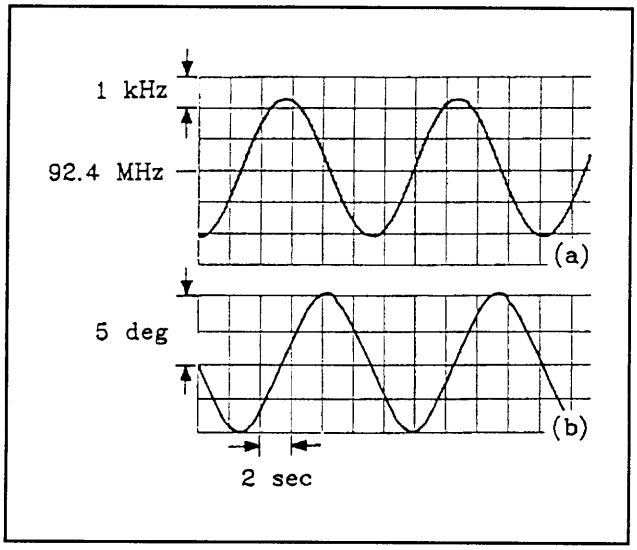

Figure 12. (a) SBS laser difference frequency with applied rotation and (b) the corresponding rotation angle for SBS gyro using SBS lasers with widely separated frequencies.

[20] S. Ezekiel, J.L. Davis, and R.W. Hellwarth, "Observation of Intensity-Induced Nonreciprocity in a Fiber Optic Gyroscope," *Opt. Lett.* 7: 457 (1982).

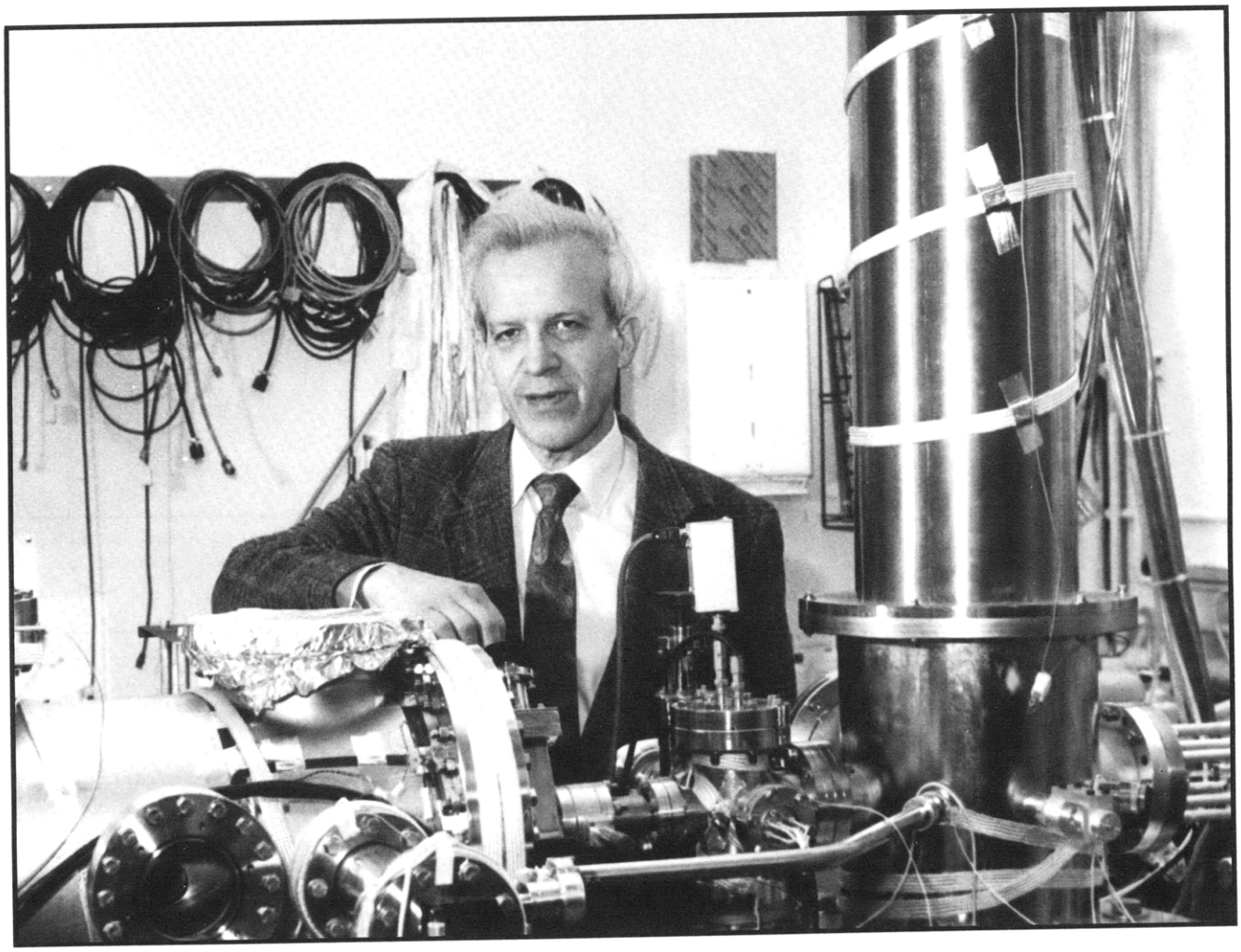

Professor Daniel Kleppner